

## ARTICLE OPEN

## An external quantum efficiency of &gt;20% from solution-processed poly(dendrimer) organic light-emitting diodes

Fatemeh Maasoumi<sup>1</sup>, Ross D. Jansen-van Vuuren<sup>1</sup>, Paul E. Shaw<sup>1</sup>, Emma V. Puttock<sup>1</sup>, Ravi Chandra Raju Nagiri<sup>1</sup>, Jake A. McEwan<sup>1</sup>, Mark Bown<sup>2</sup>, Jenny L. O'Connell<sup>2</sup>, Christopher J. Dunn<sup>2</sup>, Paul L. Burn<sup>1</sup> and Ebinazar B. Namdas<sup>1</sup>

Controlling the orientation of the emissive dipole has led to a renaissance of organic light-emitting diode (OLED) research, with external quantum efficiencies (EQEs) of >30% being reported for phosphorescent emitters. These highly efficient OLEDs are generally manufactured using evaporative methods and are comprised of small-molecule heteroleptic phosphorescent iridium(III) complexes blended with a host and additional layers to balance charge injection and transport. Large area OLEDs for lighting and display applications would benefit from low-cost solution processing, provided that high EQEs could be achieved. Here, we show that poly(dendrimer)s consisting of a non-conjugated polymer backbone with iridium(III) complexes forming the cores of first-generation dendrimer side chains can be co-deposited with a host by solution processing to give highly efficient devices. Simple bilayer devices comprising the emissive layer and an electron transport layer gave an EQE of >20% at luminances of up to  $\approx 300$  cd/m<sup>2</sup>, showing that polymer engineering can enable alignment of the emissive dipole of solution-processed phosphorescent materials.

npj Flexible Electronics (2018)2:27; doi:10.1038/s41528-018-0038-9

## INTRODUCTION

In recent years the efficiency of organic light-emitting diodes (OLEDs) has undergone a step change with the discovery that it is possible to align the emissive dipoles of phosphorescent emitters so as to enable increased light out-coupling from the device front. There are now an increasing number of reports of phosphorescent iridium(III) complex-based OLEDs with external quantum efficiencies (EQEs) greater than the theoretical limit of 20% based on the refractive indices of the materials without the use of device architecture light extraction strategies.<sup>1–4</sup> Emissive dipole alignment has also been investigated for thermally activated delayed fluorescence (TADF) emitters, with EQEs of greater than 20% now also being reported.<sup>5,6</sup> In the case of the iridium(III) complex-based phosphorescent emitters, the highly efficient devices are almost exclusively manufactured by evaporation and feature multilayer architectures and guest–host combinations to maximise and balance charge injection, charge transport, charge recombination and emission. Several criteria have been proposed to achieve emissive dipole alignment including: first, the use of heteroleptic iridium(III) complexes [e.g., Ir(ppy)<sub>2</sub>acac gives nonisotropic emission whereas the emission of Ir(ppy)<sub>3</sub> is reported to be isotropic],<sup>7–9</sup> second, the correct choice of host such that the interaction between the emitter and the host leads to dipole alignment,<sup>10,11</sup> and finally, the complexes should be processed by evaporation, with solution processing of the same complex typically giving rise to isotropic emission.<sup>8</sup> For the manufacturing of large area OLEDs, particularly for lighting, it would be advantageous to have solution-processed emissive layers that have the emissive dipole aligned in order to enhance the out-coupling of the generated light. Transition dipole alignment has been achieved for solution processed fluorescent materials.<sup>12–15</sup> However, the efficiency of

OLEDs featuring fluorescent emitters is limited by the spin statistics that lead to the generation of singlet excitons (25%), and, hence, is typically less than that of devices comprised of phosphorescent or TADF-based emitters that can exploit both the singlet and triplet excitons (100%). There has been a recent report of solution processed phosphorescent OLEDs with EQEs greater than 20%.<sup>16</sup> The OLEDs contain a graded hole injection layer, an emissive layer comprised of the emitter, hole and electron transport materials, with an additional electron transport layer (ETL) between the emissive layer and the cathode. Remarkably, the high EQEs were observed for both a homoleptic isotropic emitter [Ir(ppy)<sub>3</sub>] as well as two heteroleptic complexes, with the results somewhat at odds with previously published work on dipole alignment for enhanced emission.<sup>7–9</sup> Although no device luminances were reported, the authors comment that the high EQEs could at least be in part due to a weak optical cavity effect.

In this article, we show that poly(dendrimer)s provide a materials-based pathway for the development of efficient solution-processed OLEDs. We report that a poly(dendrimer) comprised of a norbornenyl-derived polymer backbone and first-generation iridium(III) complex-cored dendrimer side chains can give rise to simple bilayer OLEDs with efficiencies of >20%.

## RESULTS

## Light-emitting materials

The chemical structures of the singly dendronised dendrimer (**D1**) and poly(dendrimer) (**P1**) investigated in this work are shown in Fig. 1a, with the synthesis of **P1** described in the Supporting information. **D1** is a first-generation dendrimer with a homoleptic fac-(2-phenylpyridyl)iridium(III) core and fluorenyl-carbazole-

<sup>1</sup>Centre for Organic Photonics & Electronics (COPE), School of Chemistry & Molecular Biosciences and School of Mathematics & Physics, University of Queensland, St. Lucia, QLD 4072, Australia and <sup>2</sup>CSIRO Manufacturing, Research Way, Clayton, VIC 3168, Australia  
Correspondence: Paul L. Burn (paul.burn@uq.edu.au)

Received: 2 November 2017 Revised: 20 June 2018 Accepted: 3 July 2018

Published online: 23 October 2018

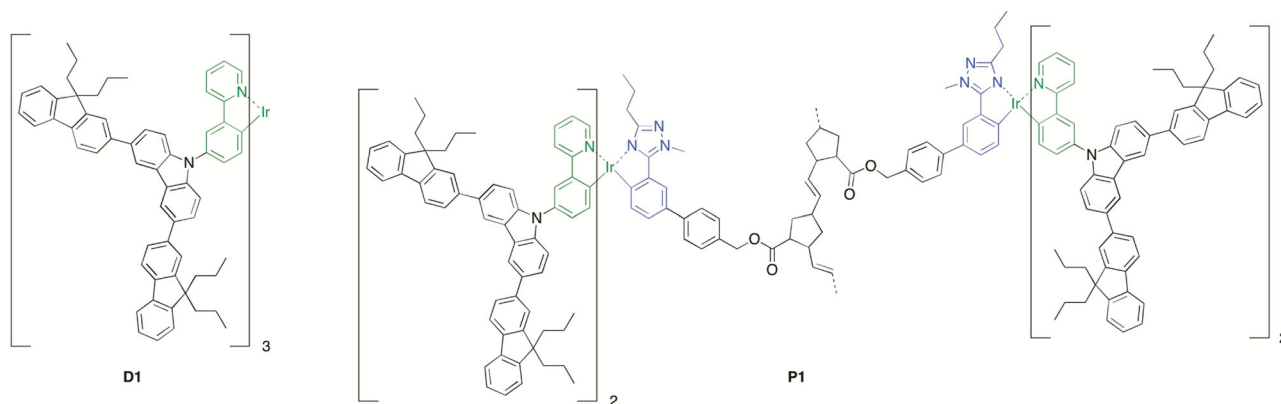


**Fig. 1** Chemical structures. Singly dendronised dendrimer **D1** and poly(dendrimer) **P1**. Both materials have carbazole-containing first-generation dendrons attached to 2-phenylpyridyl ligands, which give rise to green emission from the iridium(III) complex. **P1** is a homopolymer with a dendrimer attached to each ‘monomer’ unit of the polymer backbone, with two units shown

containing dendrons,<sup>17</sup> and provides an important comparative material for the poly(dendrimer). Such carbazolyl-containing dendrons have previously been shown to provide improved hole transport for light-emitting dendrimers,<sup>18</sup> and so were an integral part of the poly(dendrimer) design. In the case of **P1**, the iridium(III) complex core is heteroleptic, with two 2-phenylpyridyl ligands and a 1-methyl-5-phenyl-3-*n*-propyl-1*H*-[1,2,4]triazolyl co-ligand. As in the case of **D1**, the 2-phenylpyridyl ligands have the first-generation carbazole-containing dendrons attached and the phenyltriazolyl co-ligand provides the means of attachment to the polymer backbone. The norbornenyl-derived 1,3-divinylcyclopentane-polymer backbone was chosen as it could be formed by ring opening metathesis polymerisation to give materials with bulky dendritic side groups of high-molecular weight and relatively low polydispersity.<sup>19,20</sup> Gel permeation chromatography against poly(styrene) standards showed **P1** had an *M<sub>w</sub>* and dispersity of  $1.6 \times 10^5$  Da and 1.3, respectively, and it is interesting to note that based on the number average molecular weight of the polymer and monomer, the degree of polymerisation can be calculated as  $\approx 55$  units, which would correspond to a polymer length (assuming an extended polymer chain) of  $\approx 50$  nm. Furthermore, it should be noted that **P1** is a homopolymer, that is, every ‘monomer’ unit along the polymer backbone has a dendrimer attached.

#### Photophysical properties

The photophysical properties of **D1** and **P1** were first compared to determine whether there was any effect on the luminescence properties caused by linking the dendrimers via the polymer backbone. Figure 2 shows the normalised PL spectra for **D1** and **P1** in solution, neat films, and when blended at 20 wt% with 4,4'-bis(*N*-carbazolyl)biphenyl (CBP)—the host used in the subsequent device studies. It can be seen in Fig. 2a that the solution photoluminescence spectra of **D1** and **P1** are identical in spite of **D1** having a homoleptic core complex and **P1** containing a heteroleptic complex. In heteroleptic complexes such as those found in **P1**, emission effectively occurs from the ligand with the smallest optical gap.<sup>21</sup> The homoleptic complexes *fac*-tris(2-phenylpyridyl)iridium(III) [Ir(ppy)<sub>3</sub>] and *fac*-tris(1-methyl-5-phenyl-3-*n*-propyl-1*H*-[1,2,4]triazolyl)iridium(III) emit green<sup>22</sup> and blue<sup>23</sup> light, respectively, and hence the emission from both **D1** and **P1** is green (emission peak at 520 nm and a shoulder at 548 nm) with Commission Internationale de L'Éclairage (CIE) 1931 chromaticity coordinates of (0.37, 0.54). There is little change in the PL spectra in moving from solution to the solid state (Fig. 2a), indicating that the dendrons are sufficient to inhibit strong interchromophore interactions and potential aggregate or excimer formation. It should be noted that the blend film PL spectra had a small

component at 385 nm, which was due to the host material (CBP), and indicates that incomplete energy transfer has occurred in the photoluminescence experiment. The solution photoluminescence quantum yield (PLQY) of **D1** and **P1** were similar at  $82 \pm 8\%$  and  $72 \pm 7\%$ , respectively. Time-resolved PL measurements in solution (see Supplementary Fig. S1) show that both **D1** and **P1** had single exponential decays with an excited state lifetime of 1.7 and 1.5  $\mu$ s, respectively, indicating that only one type of emissive species was present. This is strong evidence that, in spite of the relative closeness of the chromophores attached to the polymer backbone, interchromophore interactions do not lead to significant quenching of the luminescence. In the solid state the PLQY values of the neat films were  $20 \pm 3\%$  for **D1** and  $30 \pm 4\%$  for **P1**, indicating that additional non-radiative decay pathways have emerged from intermolecular interchromophore interactions. This hypothesis is supported by time-resolved PL measurements, which showed that the PL decay for both **D1** and **P1** was faster than in solution and could be described in terms of two decay lifetimes of 0.2  $\mu$ s and 0.7  $\mu$ s (see Supplementary Table S1). When **D1** and **P1** were blended with CBP at 20 wt% there was an increase in the film PLQY, with the values ( $68 \pm 8\%$  for **D1**:CBP and  $71 \pm 8\%$  for **P1**:CBP) returning close to those measured in solution. The PL decays of the CBP blends were closer to those measured in solution with the main decay component having a lifetime of  $\sim 1.5 \mu$ s (see Supplementary Table S1). This confirms that intermolecular interactions are the main source of non-radiative decay for **D1** and **P1** in the neat film, but that these interactions can be effectively suppressed by blending with a host such as CBP and suggests that both **D1** and **P1** are reasonably dispersed within the host.

To gain insight into the structure of the CBP:**P1** light-emitting film we measured the surface morphology using atomic force microscopy (AFM) and the distribution of **P1** in the host using neutron reflectometry. AFM showed that the surface of the film deposited onto indium–tin oxide (ITO) was smooth with a root mean square roughness of around 0.4 nm (Fig. S2). The neutron reflectivity profiles and scattering length density versus distance from substrate plots are shown in Fig. S3. Deuterated CBP (*d*-CBP) was used to provide contrast with the protonated **P1** (deuterated materials have a higher SLD) and it was found that there was a shallow SLD gradient across the film. The SLD at the interface with the substrate was  $(3.98 \pm 0.01) \times 10^{-6} \text{ \AA}^{-2}$  with that at the upper air interface being  $(4.28 \pm 0.01) \times 10^{-6} \text{ \AA}^{-2}$ . That is, the results suggest the light-emitting layer in the device is slightly enriched with **P1** near the substrate and CBP at the interface with the ETL but overall there was no significant vertical phase separation with respect to the substrate. The relatively uniform mixing observed in

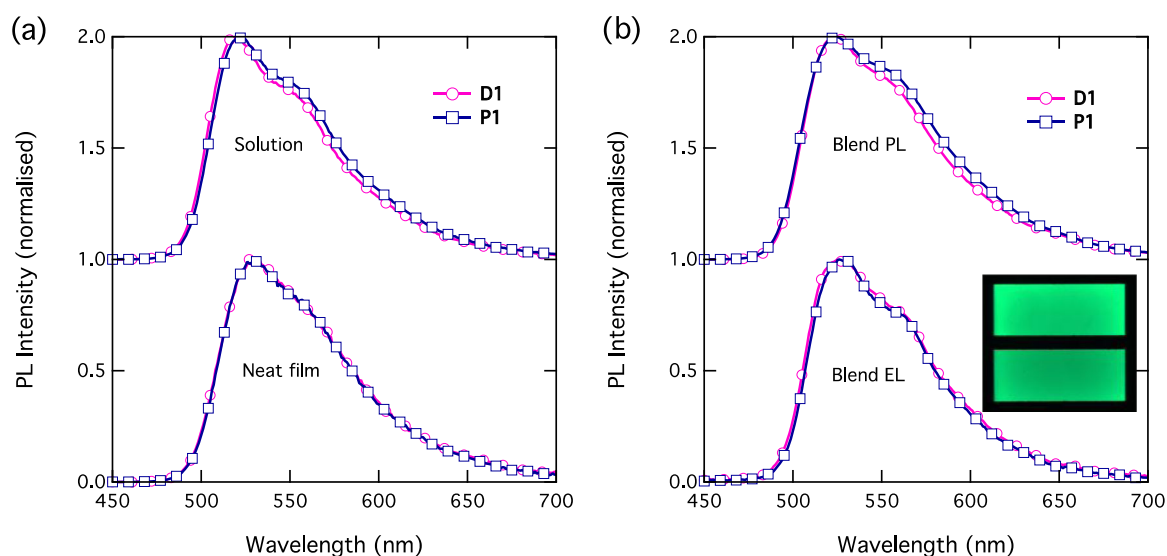


**Fig. 2** Photoluminescence and electroluminescence spectra. **a** Normalised PL spectra of **D1** and poly(dendrimer) **P1** for optically dilute solutions and neat films. **b** The PL and electroluminescence spectra of 20 wt% blends of **D1** and **P1** in CBP. Inset is a photo of two **P1**:CBP devices. The spectra are offset vertically for clarity. The samples were excited at 372 nm for the PL measurements

**Table 1.** Summary of device performance and out-coupling of the OLEDs containing a neat emissive layer and when **D1** or **P1** were blended at a concentration of 20 wt% in CBP

Device performance				Best device performance			
Material	Average EQE (%) <sup>a</sup> @ 100 cd/m <sup>2</sup>	Average Power Efficiency (lm/W) @ 100 cd/m <sup>2</sup>	Average turn on voltage <sup>b</sup> (V)	Max. EQE (%) <sup>a,c</sup>	Luminance @ max. EQE (cd/m <sup>2</sup> )	Film PLQY (%)	Out-coupling (%)
<i>Neat</i>							
<b>D1</b>	3.9 ± 0.9	8.9 ± 0.2.2	4.0 ± 0.1	4	90	20 ± 3	20 ± 3
<b>P1</b>	6.6 ± 0.5	13.2 ± 1.2	5.1 ± 0.1	7	98	30 ± 4	23 ± 3
<i>20 wt% in CBP/TPBi</i>							
<b>D1</b>	12.6 ± 1.9	24.8 ± 3.9	5.2 ± 0.3	16	57	68 ± 8	24 ± 3
<b>P1</b>	12.2 ± 2.1	25.8 ± 4.4	4.9 ± 0.3	24	33	71 ± 8	33 ± 3
<i>20 wt% in CBP/TmPyPB</i>							
<b>P1</b>	16.4 ± 2.9	34.3 ± 6.4	4.8 ± 0.3	30	30	71 ± 8	42 ± 3

<sup>a</sup>The EQE of the devices was based on the light emitted from the front of the device assuming Lambertian emission  
<sup>b</sup>Defined as a luminance of 5 cd/m<sup>2</sup>  
<sup>c</sup>The maximum EQE is quoted for a luminance of greater or equal to 30 cd/m<sup>2</sup>. The neat film performance metrics was obtained from 3 to 6 pixels on one substrate, with the blend data quoted from 12 pixels on 2 substrates for TPBi and 6 pixels on one substrate for TmPyPB

the neutron reflectometry experiment is consistent with the photophysical measurements.

#### Device performance

We next prepared bilayer devices with the structure ITO/PEDOT:PSS/emissive layer/ETL/LiF/Al [ITO = indium–tin oxide, PEDOT:PSS = poly(3,4-ethylenedioxythiophene):poly(styrenesulfonate), ETL = 1,3,5-tris(*N*-phenylbenzimidazol-2-yl)benzene (TPBi) or 1,3,5-tris(*m*-pyrid-3-yl-phenyl)benzene (TmPyPB), LiF = lithium fluoride, Al = aluminium] where the emissive layer was deposited from solution either as a neat film of the emissive material or as a 20 wt% blend with CBP. The device performance characteristics are summarised in Table 1 with the electroluminescence spectra shown in Fig. 2b. The devices with the neat emissive layer and TPBi as the ETL had modest performance with turn on voltages of around 4–5 V (defined as the voltage at which 5 cd/m<sup>2</sup> was measured). The maximum EQE for **D1** was 4% at 90 cd/m<sup>2</sup> and the device reached a maximum luminance of near 10,000 cd/m<sup>2</sup> at around 8 V (Fig. S4). The OLEDs with a neat emissive layer of **P1** reached a similar

maximum luminance to the model dendrimer, but had a slightly higher EQE (7%) at similar luminance (Fig. S4).

The devices with a blended emissive layer and TPBi ETL showed a different level of performance (Fig. 3). Although the turn on voltages were slightly higher for the **D1**:CBP blend and lower for the **P1**:CBP blend, the key result was that in both cases the EQE was significantly higher than for the OLEDs containing the neat films (Table 1). The best **D1**:CBP device (Fig. S5) had a maximum EQE of 16% at a luminance of over 50 cd/m<sup>2</sup>, but more interestingly the EQE of the best **P1**:CBP blend device was 24% at 33 cd/m<sup>2</sup> and it had a power efficiency of almost 54 lm/W (Fig. 3b). To confirm that the high EQE observed for the **P1**:CBP-based OLED was not limited to a single device architecture we changed the ETL to TmPyPB while keeping the rest of the structure the same. A slightly higher efficiency (30%) but at around the same luminance (30 cd/m<sup>2</sup>) was observed for the TmPyPB device (Fig. 3d). It should be noted that in all cases the electroluminescence spectra were similar to that of the photoluminescence (although there was no host emission) indicating that emission originates

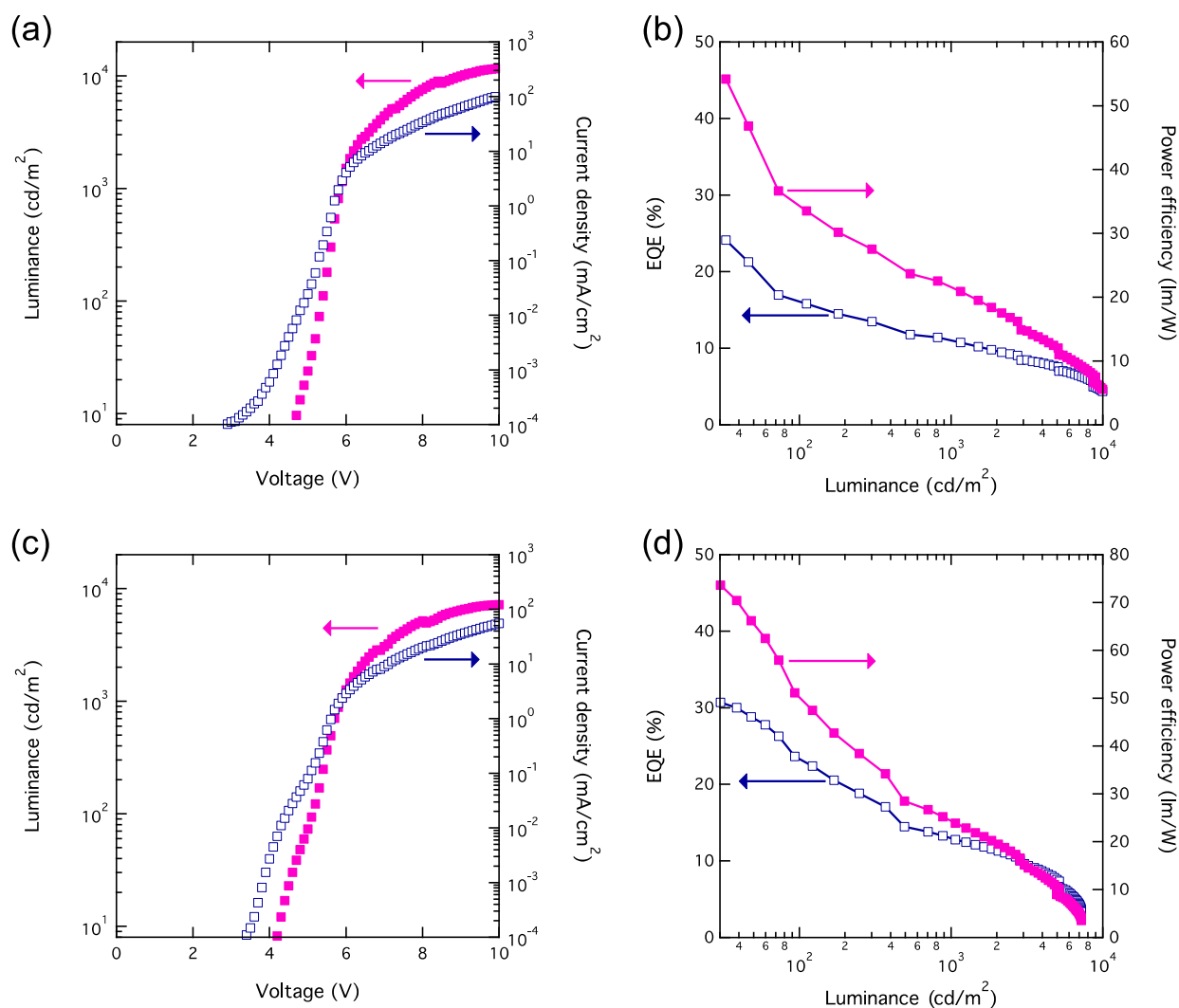


**Fig. 3** Device characteristics for the best OLEDs. **a** J–V–L curves of a device comprising a 20 wt% **P1**:CBP light-emitting layer with a TPBi ETL. **b** EQE and power efficiency as a function of the luminance of a device comprising a 20 wt% **P1**:CBP light-emitting layer with a TPBi ETL. **c** J–V–L curves of a device comprising a 20 wt% **P1**:CBP light-emitting layer with a TmPyPB ETL. **d** EQE and power efficiency as a function of the luminance of a device comprising a 20 wt% **P1**:CBP light-emitting layer with a TmPyPB ETL

from the same chromophore (Fig. 2b) and suggestive that there were no strong optical cavity effects. In addition, the emission was green with CIE coordinates of (0.37, 0.54) at 1 mA/cm<sup>2</sup>.

Finally, we measured the angular dependence of the OLED emission from neat and blend films of **D1** and **P1** (Fig. 4).

## DISCUSSION

The EQE of an OLED is given by:

$$EQE = \eta_{PLQY} \eta_{charge\ capture} \eta_{S-T} \eta_{out} \quad (1)$$

where  $\eta_{PLQY}$  is the solid-state PLQY of the emissive layer,  $\eta_{charge\ capture}$  is the efficiency of electron and hole capture to form an exciton, which is also reliant on the number of hole and electrons injected (ideally balanced),  $\eta_{S-T}$  is the singlet-triplet exciton ratio, and  $\eta_{out}$  is the efficiency of out-coupling of light from the front of the device. For a standard bottom-emitting device using an ITO-on-glass anode with an isotropic emitter,  $\eta_{out}$  is generally 20% due to the refractive indices of the materials. Thus, for perfect fluorescent and phosphorescent devices with an isotropic emitter the maximum EQE are 5% and 20%, respectively. For EQEs greater than these values, then at least one other factor needs to be in play, e.g., triplet-triplet annihilation to form additional singlet

excitons for fluorescent materials to increase  $\eta_{S-T}$  or alignment of emissive dipoles to increase  $\eta_{out}$  to above 20%. There are now a number of clear examples of phosphorescent OLEDs formed using evaporative techniques where dipole alignment of the emitter in the blended emissive layer has led  $\eta_{out}$  to be greater than 20%. Such devices include multiple layers and materials to balance charge injection and transport. In contrast, up to recently it has only been solution processed linear fluorescent emitters that have shown emissive dipole alignment for enhanced light out-coupling from thin film-based OLEDs. It has generally been thought that enhanced out-coupling by dipole alignment of solution-processed phosphorescent emitters and layers would not be possible.<sup>8</sup> The recent publication on high efficiency solution processed small-molecule phosphorescent OLEDs reported that the devices comprising the homoleptic Ir(ppy)<sub>3</sub> complex had EQEs greater than 20%.<sup>16</sup> Given the preponderance of reports that state Ir(ppy)<sub>3</sub> is an isotropic emitter, the higher EQE must be due to an optical cavity effect.

In this work, we have also considered the out-coupling of the light generated in the device for both the neat and blended emissive films. The neat film of **D1** had a PLQY of 20 ± 3% and the corresponding device had an EQE of 4%. Assuming balanced charge injection and transport, and a charge capture/



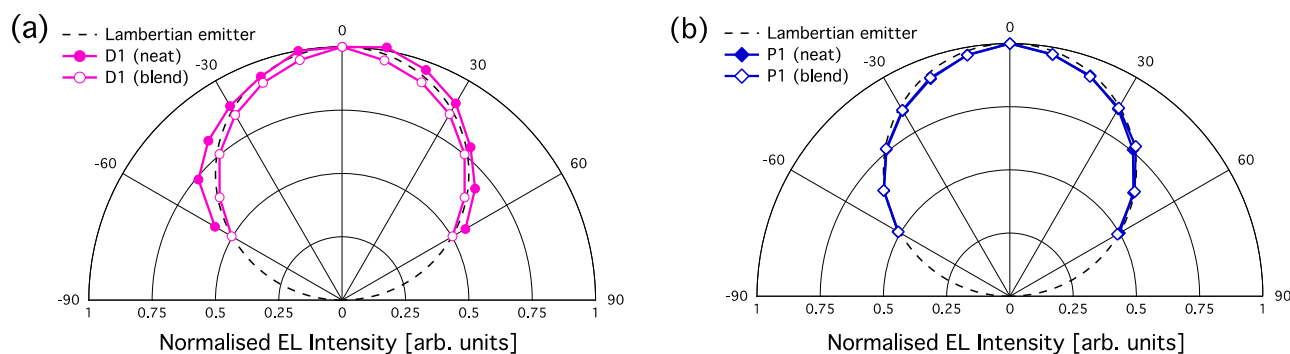


**Fig. 4** Angular dependence of the device emission. **a** OLEDS containing a neat or 20 wt% **D1**:CBP light-emitting layer and a TPBi ETL. **b** OLEDS containing a neat or 20 wt% **P1**:CBP light-emitting layer and a TPBi ETL. In all cases the emission is essentially Lambertian

recombination efficiency of one, the EQE corresponds to an out-coupling efficiency of around 20%. Similarly, for the neat films of **P1** the PLQY and maximum EQE are  $30 \pm 4$  and 7%, respectively, which within experimental error also leads to a calculation of an effective out-coupling efficiency of 20%. That is, the devices with neat emissive layers fit with the standard OLED analysis in that out-coupling is dependent on the refractive indices of the materials (the refractive indices for the blend layers are shown in Fig. S6) and there is no preferential emissive dipole alignment. Likewise, the out-coupling from the OLED comprising the homoleptic **D1**:CBP blend and a TPBi ETL is consistent with an isotropic emitter (Table 1). In contrast, the best **P1**:CBP devices had out-coupling efficiencies of greater than 20%, independent of the ETL layer that was used. Based on equation 1, the **P1**:CBP blend-based bilayer OLEDs have been calculated to have an  $\eta_{out}$  of up to  $\approx 40\%$  based on the EQE measured at  $30 \text{ cd/m}^2$ . As in the analysis for the neat and **D1**:CBP blend devices,  $\eta_{out}$  was again calculated on the basis that  $\eta_{charge \text{ capture}}$  and  $\eta_{S-T}$  were both 100%, with the measured PLQYs of the blend films setting the maximum limit. The roll-off in efficiency at higher luminance suggests that charge injection [see energy level diagram—Fig. S7] and transport, and exciton management need to be further optimised. However, the key result is that the poly(dendrimer), **P1**, can give rise to OLEDs with an EQE of >20% at viewable brightness. In order to confirm that the high EQEs and out-coupling were not simply due to device architecture and allow direct comparison with previously reported high efficiency devices we measured the angular dependence of the emission. We found that within experimental error the emission from the OLEDs was Lambertian and hence there were no optical affects arising from the device architecture that enhanced the emission. Taking these points into account it is thus reasonable to conclude that the high EQE for the best **P1**:CBP blend devices and large  $\eta_{out}$  is indicative of preferential emissive dipole alignment. **P1** is comprised of heteroleptic dendronised complexes attached to the polymer backbone and has a molecular weight that corresponds to a polymer length (assuming a linear material)<sup>24</sup> of similar magnitude to the thickness of the active layer, which could be the reason for the horizontal alignment of the emissive dipole in the blend film.

In conclusion, solution-processable phosphorescent poly(dendrimer)-based materials comprised of hole-transporting carbazole-based dendrons and iridium(III) complex-cored dendrimers have been shown to have enhanced out-coupling in standard bottom-emitting OLEDs. The poly(dendrimer) in which the dendrimers were attached as side chains on a non-conjugated polymer backbone had an out-coupling efficiency of up to around 40% and EQE of >20% at viewable brightness. The results show that solution processed macromolecular phosphorescent iridium(III) complex-based emitters can also be designed with optimised emissive dipole alignment, which is an important step forward for printing large area OLEDs, and, in particular, OLED lighting.

## METHODS

### Photoluminescence measurements

Neat films of **D1** and **P1** were made by spin-coating 20 mg/mL solutions made with spectroscopic grade chlorobenzene onto fused silica substrates to give films with thicknesses of about 50–80 nm. Blend films were made by spin-coating 20 mg/mL solutions of 20 wt% of **D1** or **P1** and CBP (Lumtec). The photoluminescence spectra were measured using a Jobin-Yvon Fluoromax 4 fluorimeter. Samples were excited at 372 nm. The thin film PLQY measurements at room temperature were performed using the method described by Greenham et al.<sup>25</sup> Solution samples were made with the materials dissolved in spectroscopic toluene and were degassed by three freeze–pump–thaw cycles before measurements. The solution PLQY was measured following the relative method<sup>26</sup> against quinine sulphate in 0.5 M  $\text{H}_2\text{SO}_4$ , which has a PLQY of 55% when excited at 360 nm. Both the reference and sample solutions had an optical density of  $\approx 0.1$ .

### Device fabrication

The OLEDs were fabricated in a Class 1000 cleanroom. The glass substrate with a pre-patterned ITO anode (160 nm,  $10 \Omega/\text{sq}$ ) from Asahi Glass Company and patterned by Techno Print Co. Ltd. was pre-cleaned with 2-propanol and water and then treated with UV-ozone for 15 min at 25 °C immediately prior to use. The devices had the following layer structure glass/ITO(160 nm)/PEDOT:PSS(40 nm)/emissive layer ( $\approx 50$ –80 nm)/TPBi or TmPyPB (35 nm)/LiF (1 nm)/Al (100 nm). PEDOT:PSS (Heraeus, AI 4083) was spin-coated onto the cleaned ITO and annealed for 15 min at 150 °C. The devices were then transferred into a nitrogen-filled glovebox where the emissive layer (neat or blend) was deposited onto the PEDOT:PSS by spin-coating from chlorobenzene (for the neat films) or chloroform (for the blends with CBP) solution at a concentration of 20 mg/mL where the blend solution consisted of 20 wt% dopant. The thickness of the emissive layers was measured with a Dektak profilometer with neat **D1** being  $55 \pm 5$  nm and **P1**  $75 \pm 5$  nm, and 20 wt% **D1**:CBP and **P1**:CBP being  $55 \pm 5$  nm and  $65 \pm 5$  nm, respectively. TPBi (Lumtec), TmPyPB (Lumtec) LiF, and Al were deposited by thermal evaporation through shadow masks in a vacuum chamber with a base pressure of around  $5 \times 10^{-6}$  Pa. The TPBi deposition rate was maintained at approximately  $1 \text{ \AA/s}$ . After the organic layer was deposited, the cathode layers, LiF ( $\approx 1$  nm) and Al (100 nm), were deposited using a second shadow mask without breaking the vacuum, resulting in a device design of six  $2 \text{ mm} \times 5 \text{ mm}$  pixels per substrate. Completed devices were transferred under an inert atmosphere from the vacuum chamber to a glovebox (water and oxygen concentration levels  $< 0.1$  ppm) for encapsulation with a glass cover using UV-cured epoxy resin and an adhesive desiccant. Encapsulated devices were then transferred outside the glovebox for characterisation.

### Device characterisation

The J–V–L measurements were performed using a Keithley 2400 sourcemeter and a Topcon Luminance Colorimeter BM-7A with a measuring (or light acceptance) cone angle of  $0.2^\circ$ . The calibration of the measurement is described in the Supporting information. Measurements were made at normal incidence, with the nose of the colour camera held approximately 40 cm from the sample by collecting collimated light captured from a circular measuring spot with a diameter of  $\sim 1$  mm that appeared in the viewfinder of the camera. The EQEs shown in Fig. 3b, d at  $30 \text{ cd/m}^2$  are likely underestimated by around a few percent (see Supporting information). To

setup the test on each pixel successively, the sample was moved under the camera so that the measuring spot fell entirely within the particular single pixel under test, before the pixel was driven and the J–V–L dataset acquired for that pixel. An ASEQ LR1 mini-spectrometer was used to measure the EL spectra of devices at normal incidence from which the EQE was calculated, in conjunction with the same Keithley 2400 sourcemeter. The angle-dependent EL intensity measurements were performed with a Minolta LS-110 luminance meter between normal incidence and  $\pm 60^\circ$  in steps of  $10^\circ$ . The devices were driven with a constant current of 100  $\mu\text{A}$  with a Keithley 2400 for the duration of the measurement. The data were corrected for the change in the measurement spot size with angle and normalised to the luminance value at normal incidence.

## DATA AVAILABILITY

The datasets generated during and/or analysed during the current study are available from the corresponding author on reasonable request.

## ACKNOWLEDGEMENTS

P.L.B. is an ARC Laureate Fellow (FL160100067). E.B.N. is the recipient of a UQ Fellowship. P.E.S. is an Advance Queensland Research Fellow. F.M. was funded by a University of Queensland International Scholarship and E.V.P. is supported by the Australian Research Council (DP170102077). We would like to thank Dr. Dani Stoltzfus for carrying out the PESA measurements. We acknowledge support from the University of Queensland (Strategic Initiative—Centre for Organic Photonics & Electronics). We thank Professor Ian Gentle and Drs. Andrew Clulow and Andrew Nelson for assistance with the neutron reflectometry measurements and Jaber Saghaei for the Atomic Force Microscopy Image.

## AUTHOR CONTRIBUTIONS

P.L.B. designed the concept and initiated the programme with F.M. and R.V.V. contributing equally to the experimental results. R.V.V. and E.V.P. prepared and analysed the materials. F.M. fabricated and characterised the devices, undertook the photophysical measurements, and analysed the results. P.E.S. contributed to the interpretation of the photophysical results and performed the OLED angular dependence measurements. J.A.M. performed and analysed the neutron reflectometry measurements. M.B., J.O.'C. and C.D. (CSIRO) provided the device fabrication tooling and measurement techniques. EBN and PLB supervised the project and all authors contributed to the manuscript preparation.

## ADDITIONAL INFORMATION

**Supplementary Information** accompanies the paper on the *npj Flexible Electronics* website (<https://doi.org/10.1038/s41528-018-0038-9>).

**Competing interests:** The authors declare no competing interests.

**Publisher's note:** Springer Nature remains neutral with regard to jurisdictional claims in published maps and institutional affiliations.

## REFERENCES

1. Tanaka, D. et al. Ultrahigh efficiency green organic light-emitting devices. *Jpn. J. Appl. Phys.* **46**, L10 (2006).
2. Lee, C. W. & Lee, J. Y. Above 30% external quantum efficiency in blue phosphorescent organic light-emitting diodes using pyrido [2,3-b] indole derivatives as host materials. *Adv. Mater.* **25**, 5450–5454 (2013).
3. Park, Y. S. et al. Exciplex-forming co-host for organic light-emitting diodes with ultimate efficiency. *Adv. Funct. Mater.* **23**, 4914–4920 (2013).
4. Kim, K.-H., Ahn, E. S., Huh, J.-S., Kim, Y.-H. & Kim, J.-J. Design of heteroleptic Ir complexes with horizontal emitting dipoles for highly efficient organic light-emitting diodes with an external quantum efficiency of 38%. *Chem. Mater.* **28**, 7505–7510 (2016).
5. Oh, C. S. et al. Relationship between molecular and dipole orientation of thermally activated delayed fluorescent emitters. *Org. Electron.* **42**, 337–342 (2017).

6. Kaji, H. et al. Purely organic electroluminescent material realizing 100% conversion from electricity to light. *Nat. Commun.* **6**, 8476 (2015).
7. Jurow, M. J. et al. Understanding and predicting the orientation of heteroleptic phosphors in organic light-emitting materials. *Nat. Mater.* **15**, 85–91 (2016).
8. Lampe, T. et al. Dependence of phosphorescent emitter orientation on deposition technique in doped organic films. *Chem. Mater.* **28**, 712–715 (2016).
9. Graf, A. et al. Correlating transition dipole moment orientation of phosphorescent emitter molecules in OLEDs with basic materials properties. *J. Mater. Chem. C* **2**, 10298–10304 (2014).
10. Moon, C.-K., Kim, K.-H., Lee, J. W. & Kim, J.-J. Influence of host molecules on emitting dipole orientation of phosphorescent iridium complexes. *Chem. Mater.* **27**, 2767–2769 (2015).
11. Kim, K.-H. et al. Phosphorescent dye-based supramolecules for high-efficiency organic light-emitting diodes. *Nat. Commun.* **5**, 4769 (2014).
12. Senes, A. et al. Transition dipole moment orientation in films of solution processed fluorescent oligomers: investigating the influence of molecular anisotropy. *J. Mater. Chem. C* **4**, 6302–6308 (2016).
13. Zhao, L. et al. Horizontal molecular orientation of light-emitting oligofluorenes in spin-coated glassy organic thin films. *J. Mater. Chem. C* **4**, 11557–11565 (2016).
14. Kim, K.-H. et al. Highly efficient non-doped deep blue fluorescent emitters with horizontal emitting dipoles using interconnecting units between chromophores. *Chem. Commun.* **52**, 10956–10959 (2016).
15. Zhao, L. et al. Horizontal molecular orientation in solution-processed organic light-emitting diodes. *Appl. Phys. Lett.* **106**, 063301 (2015).
16. Han, T. H. et al. Ultrahigh-efficiency solution-processed simplified small-molecule organic light-emitting diodes using universal host materials. *Sci. Adv.* **2**, e1601428 (2016).
17. Knights, K. A. et al. A rapid route to carbazole-containing dendrons and phosphorescent dendrimers. *J. Mater. Chem.* **18**, 2121–2130 (2008).
18. Gambino, S., Stevenson, S. G., Knights, K. A., Burn, P. L. & Samuel, I. D. W. Control of charge transport in iridium(III) complex-cored carbazole dendrimers by generation and structural modification. *Adv. Funct. Mater.* **19**, 317–323 (2009).
19. Lai, W.-Y. et al. Poly(dendrimers) with phosphorescent iridium(III) complex-based side chains prepared via ring-opening metathesis polymerization. *Macromolecules* **45**, 2963–2971 (2012).
20. Lai, W.-Y. et al. The 'double dendron' approach to host free phosphorescent poly(dendrimer) OLEDs. *Polym. Chem.* **3**, 734–740 (2012).
21. Frampton, M. J., Namdas, E. B., Lo, S.-C., Burn, P. L. & Samuel, I. D. W. The synthesis and properties of solution processable red-emitting phosphorescent dendrimers. *J. Mater. Chem.* **14**, 2881–2888 (2004).
22. Baldo, M. A., Lamansky, S., Burrows, P. E., Thompson, M. E. & Forrest, S. R. Very high efficiency green organic light-emitting devices based on electrophosphorescence. *Appl. Phys. Lett.* **75**, 4–6 (1999).
23. Lo, S.-C. et al. Blue phosphorescence from iridium(III) complexes at room temperature. *Chem. Mater.* **18**, 5119–5129 (2006).
24. Chen, Y. & Xiong, X. Tailoring dendronised polymers. *Chem. Commun.* **46**, 5049–5060 (2010).
25. Greenham, N. et al. Measurement of absolute photoluminescence quantum efficiencies in conjugated polymers. *Chem. Phys. Lett.* **241**, 89–96 (1995).
26. Crosby, G. A. & Demas, J. N. Measurement of photoluminescence quantum yields. *Review. J. Phys. Chem.* **75**, 991–1024 (1971).



**Open Access** This article is licensed under a Creative Commons

Attribution 4.0 International License, which permits use, sharing, adaptation, distribution and reproduction in any medium or format, as long as you give appropriate credit to the original author(s) and the source, provide a link to the Creative Commons license, and indicate if changes were made. The images or other third party material in this article are included in the article's Creative Commons license, unless indicated otherwise in a credit line to the material. If material is not included in the article's Creative Commons license and your intended use is not permitted by statutory regulation or exceeds the permitted use, you will need to obtain permission directly from the copyright holder. To view a copy of this license, visit <http://creativecommons.org/licenses/by/4.0/>.

© The Author(s) 2018